ICASSP 2024 - 2024 IEEE International Conference on Acoustics, Speech and Signal Processing (ICASSP) | 979-8-3503-4485-1/24/$31.00 ©2024 IEEE | DOI: 10.1109/ICASSP48485.2024.10445980

V-DDPM: MRI RICIAN NOISE REMOVAL MODEL BASED ON VST AND DDPM

Yue Hu[1,2] *Huiying Xu*[1,*] *Xinzhong Zhu* [1] *Hundera Negalign Wake* [1,3]

[1]School of Computer Science and Technology, Zhejiang Normal University, Jinhua, China
[2]Mechanical & Electrical Engineering College, Jinhua Polytechnic, Jinhua, China
[3]Zhejiang Institute of Optoelectronics, Jinhua, China

ABSTRACT

Magnetic resonance imaging (MRI) often contains Rician noise. Unlike additive Gaussian noise, the distribution of Rician noise is related to the data of the image, making it more difficult to remove. It has been shown that the variance stabilizing transformation (VST) can transform the Rician noise distribution into a variance stabilized Gaussian distribution. Utilizing this property, combined with the diffusion model, we proposed an algorithm for the removal of Rician noise from MRI. The algorithm first performs VST on the MRI containing Rician noise and then carries out diffusion denoising. A Gaussian noise sequence is added to the diffusion process; afterward, the diffusion process is reversed to provide different denoising levels through Markov chain modeling. Finally, the denoised image is obtained through the inverse of VST. Experimental results demonstrate the performance of our method in removing Rician noise from magnetic resonance images compared to DDPM denoising alone, while preserving detailed information better. Noise removal was also performed for MRI with a simple structure.

Index Terms— Magnetic resonance imaging, Rician noise, Noise removal, Variance stabilizing transformation, Diffusion modeling.

1. INTRODUCTION

Magnetic resonance (MR) imaging is a crucial tool in modern medicine, offering detailed images for diagnostic purposes. However, it comes with challenges including complexity and slow imaging speeds, exacerbated by noise interference that can degrade image quality. This noise not only complicates further image processing tasks such as segmentation, alignment, and visualization but also seriously affects the clinician's diagnosis [1]. Therefore, it is crucial to solve the noise problem of MR images.

Many techniques have been explored for MRI denoising, including filtering methods [2-5]. and the prevalent nonlocal means (NLM) method, which has been extended for nonlocal regions for MRI denoising [6, 7]. Liling Yu et al. introduced a promising approach that combining the BM3D algorithm and variance stabilized transform for denoising MRI and to accurately estimate the noise level of MRI and effectively remove noise in MR images [8]. Recently, advancements in deep learning have fostered innovative approaches to medical image denoising, enhancing model performance by utilizing richer contextual information from expanded regions. Jiang et al. developed a denoising convolutional neural network with multiple channels, which was validated using MRI datasets [9]. Meanwhile, Ran et al. introduced a generative adversarial network based on residual encoder-decoder architecture for denoising MRI images. This approach leverages the residual network and autoencoder to effectively preserve the image's structural details and edges [10].

Denoising diffusion probabilistic models (DDPMs) iteratively refine a normal distribution to a data-specific one through a two-step process: a forward phase that injects noise into the image, and a reverse phase that gradually removes it, creating refined data samples. This approach has successfully been applied in numerous computer vision tasks including image generation, super-resolution, and MRI reconstruction [11-13].

The variance stabilizing transformation (VST) is utilized to convert Rician noise in MRI into additive Gaussian noise, lessening noise reliance on the initial image and facilitating the handling of complex problems by transforming heteroscedastic data into homoscedastic data. In 1999, Nowak [14] proposed that mode-squaring of MRI can reduce the correlation between image data and noise, and then denoising of mode-squared images with bias correction could be conducted through filtering. In 2011, Foi [15] proposed using the VST framework to estimate and remove the Rice distribution noise in MRI.

This paper evaluates a diffusion model's efficacy in eliminating Rician noise from MRI images post-VST application. The process involves applying VST to the noisy image, denoising it is using a trained DDPM model, followed by IVST application. Results indicate enhanced image visual quality and superior denoising outcomes with this method. The performance comparison analysis shows that the new method improves the visual quality of the image and obtains a better denoising effect.

2. RICIAN NOISE OF MRI

2.1. Rician noise of MRI

MR is widely used in medical diagnosis because of its rapid imaging and less hazardous characteristics, but noise is often introduced during the imaging process. Raw MR data are collected in K-space, and the data in K-space consist of two signal parts, the real part and the imaginary part, with a phase difference of 90 degrees. Noise contained in MR images is Gaussian distributed in the complex domain [16], and through the application of computer-assisted graphical analysis, it is determined that the noise contained in the MR images obeys the Rician distribution in its entirety.

The original signal is reconstructed using the discrete Fourier inverse transform to obtain the image domain data of MR. Due to the linearity and orthogonality of the Fourier transform, the reconstructed MR image data are still complex Gaussian noise. For the subsequent image processing and visual requirements, the reconstructed data is modeled which changes the complex Gaussian distributed noise to a Rician distribution [17].

The observed MRI is the magnitude image obtained from the reconstructed data by the modulo operation,

$$|Z| = \sqrt{(r\cos\theta + n_1)^2 + (r\sin\theta + n_2)^2}, \quad (1)$$

where Z is the MRI complex signal; n_1 and n_2 are the additive Gaussian white noises with a mean value of 0, the same standard deviation and independent of each other; the amplitude and phase of the original MRI are r and θ, respectively.

The above equation shows that the noise in the modal image Z observed by MRI is no longer additive Gaussian noise but changes to a Rician distribution associated with the image data with a probability density function of

$$P(z \mid r,\sigma) = \frac{z}{\sigma^2} e^{-\frac{z^2+R^2}{2\sigma^2}} I_0(\frac{zr}{\sigma^2}), \tag{2}$$

where I_0 denotes the zero-order modified Bessel function. The inference from Eq. 3 shows that the low-intensity region of the signal-to-noise ratio (SNR) has a Rayleigh distribution, the high-intensity region of the SNR obeys a Gaussian distribution.

3. METHODS

The proposed method, termed V-DDPM, encompasses three steps: (1) variance stabilizing transformation (VST) of noisy MRI data, (2) noise removal utilizing DDPM, and (3) inverse transformation applied to the denoised MRI data.

3.1. Variance stabilizing transformation (VST)

The distribution of Rician noise is related to the image data, and its variance varies with the data. VST is an algorithm capable of converting the Rician distribution into an additive Gaussian distribution. After the VST transformation, the MRI noise is changed into a Gaussian distribution with a stable variance so that it can be denoised by a variety of filtering methods that are applicable to Gaussian noise. After that, the inverse transform of VST is performed to obtain the denoised MRI [17].

The VST algorithm formula can be defined as

$$f(Z) = \sqrt{\frac{Z^2}{\sigma^2} - \frac{1}{2}} + a, \tag{3}$$

where Z and σ have the same meaning as in Eq. 4 and a is a constant,

$$a = f(Z_{\max}) - \sqrt{\frac{Z_{\max}^2}{\sigma^2} - \frac{1}{2}}. \tag{4}$$

Let the denoising method be Φ, and the image D is obtained after denoising the image $f(Z)$, which contains additive Gaussian noise after VST conversion,

$$D = \Phi(f(Z)). \tag{5}$$

The final denoised image I can be obtained by unbiased estimation of VST inversion on D,

$$I \approx \frac{\sigma(D-a)^2}{\sqrt{(D-a)^2 + 1/2}}. \tag{6}$$

3.2. The Denoise Diffusion Probability Model (DDPM)

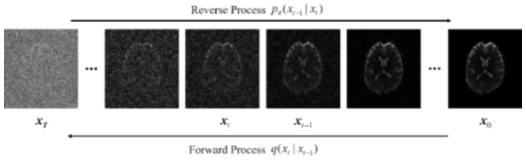

Fig. 1: Diagram of the DDPM framework.

The Denoise Diffusion Probability Model (DDPM) is a class of generative models that mainly includes two processes: a forward process and a reverse process, as shown in **Fig. 1**.

Different from generative networks such as the generative adversarial network (GAN), variational autoencoder (VAE) and normalized flow model (NFM), diffusion model progressively introduces noise into the image during the forward process until the image is corrupted into complete Gaussian noise, and then they learn to restore the image from Gaussian noise to the real image during the reverse sampling process. The diffusion model is a parameterized Markov chain throughout the processes [11].

The forward process continuously adds Gaussian noise to the image so that it gradually approaches a Gaussian distribution associated with the input data. Here, the non-noisy data are denoted as x_t, $x_t \sim q(x_0)$. $q(x_0)$ are the original data distributions not corrupted by noise; then, the relationship between the noisy state at moment t and the previous moment is:

$$q(x_t \mid x_{t-1}) = \mathcal{N}(x_t; \sqrt{1-\beta_t} \cdot x_{t-1}, \beta_t \cdot \mathbf{I}), \tag{7}$$

where $t \in \{0,1,...,T\}$, $\mathcal{N}$ denotes the Gaussian noise distribution, β_t is the noise variance modifier associated with the moment t, and $\mathbf{I}$ is a unit matrix with the same dimensions as the initial state x_0. Then, the joint distribution of $x_1, x_2, ..., x_T$ under input x_0 can be described as:

$$q(x_1, x_2, ..., x_T \mid x_0) = \prod_{t=1}^{T} q(x_t \mid x_{t-1}). \tag{8}$$

The noisy state at moment t conditional on the input x_0 can be obtained directly by Markov chain modeling as

$$q(x_t \mid x_0) = \mathcal{N}(x_t; \sqrt{\bar{\alpha}_t} \cdot x_0, (1-\bar{\alpha}_t) \cdot \mathbf{I}), \tag{9}$$

where $\alpha_t = 1 - \beta_t$, $\bar{\alpha}_t = \prod_{l=1}^{t} \alpha_l$.

According to Eq. 8, the relationship between x_t and x_{t-1} which are the noisy state at time t and time $t-1$ can be obtained as

$$x_t = \sqrt{\alpha_t} \cdot x_{t-1} + \sqrt{1-\alpha_t} \cdot \varepsilon_{t-1}, \tag{10}$$

where $\varepsilon_{t-1} \sim \mathcal{N}(\mathbf{0}, \mathbf{I})$.

The relationship between x_t and the input x_0 can be obtained by constant substitution recursion as

$$x_t = \sqrt{\bar{\alpha}_t} \cdot x_0 + \sqrt{1-\bar{\alpha}_t} \cdot \varepsilon \tag{11}$$

where $\varepsilon, \varepsilon_{t-1}, \varepsilon_{t-2} \sim \mathcal{N}(\mathbf{0}, \mathbf{I})$ and $\bar{\varepsilon}_{t-2}$ combine two Gaussian distributions. The above derivation process utilizes two Gaussian distributions with different variances $\mathcal{N}(\mathbf{0}, \sigma_1^2 \cdot \mathbf{I})$ and $\mathcal{N}(\mathbf{0}, \sigma_2^2 \cdot \mathbf{I})$ added together to equal a new Gaussian distribution $\mathcal{N}(\mathbf{0}, (\sigma_1^2 + \sigma_2^2) \cdot \mathbf{I})$.

The backward process estimates the noise distribution by learning based on the existing noisy state, further obtains the state of the previous moment, and gradually constructs the real data from the Gaussian distribution. According to the result of the forward process, the posterior distribution $p(x_t) \sim \mathcal{N}(x_t; \mathbf{0}, \mathbf{I})$ of the noisy state x_T at moment T can be considered; then, the joint distribution $p_\theta(x_1, x_2, ..., x_T)$ is also a Markov chain, which is defined as:

$$p_\theta(x_1, x_2, ..., x_T) = p(x_T)\prod_{t=1}^{T} p_\theta(x_{t-1} \mid x_t). \quad (12)$$

Then, the x_{t-1} at moment $t-1$ can be obtained from state x_t at the previous moment t, and its conditional distribution can be expressed as follows:

$$p_\theta(x_{t-1} \mid x_t) = \mathcal{N}(x_{t-1}; \mu_\theta(x_t, t), \Sigma_\theta(x_t, t)), \quad (13)$$

through the noise estimation network at time t, the mean value of noise is $\mu_\theta(x_t, t)$ and the variance is $\Sigma_\theta(x_t, t)$, and θ is the parameter of the noise estimation network.

When the input is x_0, the true conditional distribution between x_{t-1} and x_t is

$$q(x_{t-1} \mid x_t, x_0) = \mathcal{N}(x_{t-1}; \mu_t(x_t, x_0), \beta_t \cdot \mathbf{I}), \quad (14)$$

where the noise posterior distribution parameters μ_t and β_t are:

$$\mu_t = \frac{1}{\sqrt{\alpha_t}}(x_t - \frac{\beta_t}{\sqrt{1-\bar{\alpha}_t}} \cdot \varepsilon_t), \beta_t = \frac{1-\bar{\alpha}_{t-1}}{1-\bar{\alpha}_t} \cdot \beta_t. \quad (15)$$

Using the noise estimation network μ_θ to estimate the true noise distribution mean μ_t, the noise distribution mean in the above equation can be estimated as:

$$\mu_\theta(x_t, t) = \frac{1}{\sqrt{\alpha_t}}(x_t - \frac{\beta_t}{\sqrt{1-\bar{\alpha}_t}} \cdot \varepsilon_\theta(x_t, t)). \quad (16)$$

According to the formula, the noisy state x_t at moment t satisfies $x_t = \sqrt{\bar{\alpha}_t} \cdot x_0 + \sqrt{1-\bar{\alpha}_t} \cdot \varepsilon$; then, the noisy state x_{t-1} at moment $t-1$ can be described as

$$x_{t-1} = \frac{1}{\sqrt{\alpha_t}}(x_t - \frac{1-\alpha_t}{\sqrt{1-\bar{\alpha}_t}} \cdot \varepsilon_\theta(x_t, t)). \quad (17)$$

Then, according to the estimation of the noise distribution, the noise estimation network at different moments can be gradually back sampled to obtain the real data distribution based on the above equation.

4. EXPERIMENTS

4.1. Experiment Data

The data utilized in the crafting of this article were sourced from the NYU fastMRI Initiative database, accessible at fastmri.med.nyu.edu [18, 19]. While the NYU fastMRI investigators supplied the data, they did not engage in the analysis or contribute to writing of this report. A continually updated list of NYU fastMRI investigators is available at fastmri.med.nyu.edu. The foremost objective of the fastMRI initiative is to explore the potential of machine learning in assisting with the reconstruction of medical images. To verify the denoising effect of the algorithm proposed in this paper for different MR images, two MR images of different tissues were selected for denoising experiments. The selected images were knee MRI (coronal proton density-weighted images without fat suppression) and brain MRI (axial T1-weighted, T2-weighted images on 3 Tesla magnets), which were coaligned with each other and resampled to 512 × 512 pixels.

To obtain the simulated image containing Rician noise contamination, the noise-containing image Z was generated. Noise at 2%, 4%, 5%, 6% and 10% levels were added in the experiment. The MRI after adding different levels of Rician noise is shown in **Fig. 2**, where **a)** is an MRI without noise.

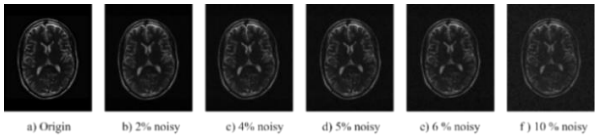

Fig. 2: MRI with different noise levels.

The noise-containing image can be represented as

$$|Z| = \sqrt{(r + \sigma \times randn(size(r)))^2 + (\sigma \times randn(size(r)))^2}, \quad (18)$$

where $\sigma = percentNoise\% \times \frac{t}{100} S_{\max}$, t denotes the proportion of noise, $S_{\max}$ denotes the maximum value of pixels in the image, $randn(size(r))$ generates data mirroring the dimensions of the original images, characterized by a mean and standard deviation of t are 0 and 1, respectively.

4.2. Evaluation

The experiments were conducted to objectively analyze the denoising effect using two performance parameters, the peak signal-to-noise ratio (PSNR) and mean structural similarity [20] (SSIM), and to compare the visual effects of the denoised images. The PSNR is defined as

$$PSNR = 10 \cdot \log_{10} \frac{S_{\max}}{\sigma_{RMSE}^2}. \quad (19)$$

The root mean square error is

$$\sigma_{RMSE} = \sqrt{\frac{1}{L}\sum_{i=1}^{L}(I_i - S_i)}, \quad (20)$$

where L is the image size of the image, S is the original image, and I is the denoised image. The average SSIM serves as a metric to quantify the level of structural resemblance between two images, with its numerical range spanning from -1 to 1. A higher value signifies a greater similarity in structure exhibited by the two images. Typically, the average SSIM of an entire image is obtained by averaging the local SSIMs within the image. Local SSIM is defined as

$$SSIM(x, y) = \frac{(2\mu_x\mu_y + c_1)(2\sigma_{xy} + c_2)}{(\mu_x^2 + \mu_y^2 + c_1)(\sigma_x^2 + \sigma_y^2 + c_2)}, \quad (21)$$

where x and y represent the localized image segments acquired through windowing of the initial and enhanced images, correspondingly, μ_x, σ_x^2 and σ_{xy} are the mean, variance and covariance within the image blocks, respectively, and c_1 and c_2 are two constants.

5. RESULTS

Table 1 shows the PSNR values of different denoising algorithms for brain MRI and knee MRI after the denoising process and gives the PSNR values of images denoised directly using NLM filtering. From **Table 1**, it can be seen that the effect of NLM denoising of MR images that contain Rician noise is poor.

However, the V-DDPM algorithm significantly improves the denoising effect compared to the NLM algorithm, and the PSNR value of the denoised image increases by about 3-7 dB.

Table 2 shows the average SSIM value of each algorithm. From the data in **Table 2**, it can be seen that the improved algorithms significantly increase the average SSIM value of the image. The quantitative comparison of the performance parameters in **Table 1** and **Table 2** illustrates that the improved algorithm using V-DDPM for denoising MRI improves the denoising effect, and the performance is significantly improved.

Table 1: PSNR comparison of different denoising methods.

Experimental images		arithmetic	noise intensity				
			2%	4%	5%	6%	10%
Brain MRI	T1 weighted	NLM	33.3325	29.4872	25.1943	24.8636	23.6427
		DDPM	35.2222	35.6652	32.3311	32.3882	30.3397
		V-DDPM	**36.7163**	**37.0754**	**33.2581**	**33.3408**	**31.4371**
	T2 weighted	NLM	35.3803	31.4159	27.2590	25.6261	23.1634
		DDPM	39.2534	36.3294	34.5555	33.2638	31.5829
		V-DDPM	**41.5381**	**37.8101**	**35.7872**	**34.3307**	**31.6997**
Knee MRI	PD	NLM	30.0282	29.2603	27.3144	25.8140	21.5747
		DDPM	34.0089	34.7506	32.8248	29.4193	26.4311
		V-DDPM	**35.3773**	**35.9246**	**33.8013**	**30.1087**	**27.5984**

Table 2: SSIM comparison of different denoising methods.

Experimental images		arithmetic	noise intensity				
			2%	4%	5%	6%	10%
Brain MRI	T1 weighted	NLM	0.7901	0.7413	0.6872	0.6867	0.5374
		DDPM	0.9705	0.9623	0.9414	0.9312	0.8820
		V-DDPM	**0.9765**	**0.9766**	**0.9573**	**0.9368**	**0.8947**
	T2 weighted	NLM	0.8089	0.7359	0.6916	0.6856	0.5853
		DDPM	0.9729	0.9686	0.9477	0.9255	0.8921
		V-DDPM	**0.9824**	**0.9733**	**0.9598**	**0.9346**	**0.9089**
Knee MRI	PD	NLM	0.7413	0.7354	0.7046	0.6992	0.5795
		DDPM	0.9579	0.8794	0.8703	0.7916	0.7524
		V-DDPM	**0.9662**	**0.8855**	**0.8789**	**0.7952**	**0.7646**

Fig. 3 contains some of the data from Table 1. **Fig. 3a)** shows the PSNR of the T2-weighted brain MRI with different noise intensity. The curve of the V-DDPM algorithm is at the top. The comparison shows that PSNR decreases with the increase of noise intensity. Moreover, it can be found that when the noise intensity is greater than 5%, the PSNR values of V-DDPM and DDPM are very close, and the VST module plays a small role. **Fig. 3b)** includes the PSNR of the PD knee MRI, the results are similar to **a)**. The difference is that the overall effect will be worse than the effect on the brain MRI.

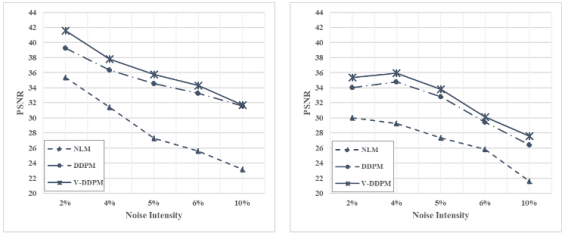

a) Brain MRI (T2-weighted) b) Knee MRI (PD)

Fig. 3: the PSNR of T2-weighted brain MRI and PD knee MRI with different noise intensity

To comparatively analyze the visual effect of denoising, **Fig. 4** show the recovered images obtained by different algorithms after denoising T2-weighted Brain MRI containing 6% Rician noise intensity. As seen from the figures, the image restoration effect of the NLM algorithm after denoising is general, and little information content is lost. Compared with them, the improved algorithm removes the noise more effectively and achieves the best visual effect, and the visible noise is obviously reduced, which indicates that the improved algorithm effectively protects the edge and detail information of the image while removing the noise, the difference from the original image is small.

According to the experimental results, from a visual point of view, **Fig. 5** shows the MRI of the human knee, which has a simple structure, little detail, and clear outline. After the V-DDPM algorithm, the noise reduction effect is better. Although it contains some noise points, the structure is clear, and the detail content recovery ability is better than other algorithms.

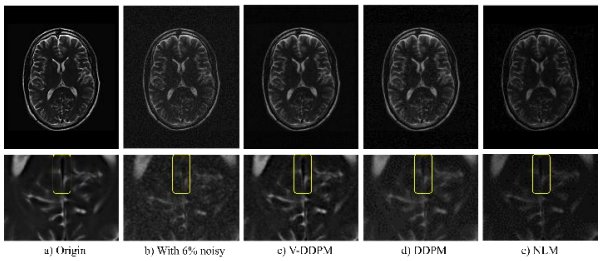

Fig. 4: Comparison of results on T2-weighted Brain MRI. The initial row showcases the entire image, while the subsequent row presents an **amplified** version of the identical region. A comprehensive comparison of detailed information is evident within the designated **yellow box** area.

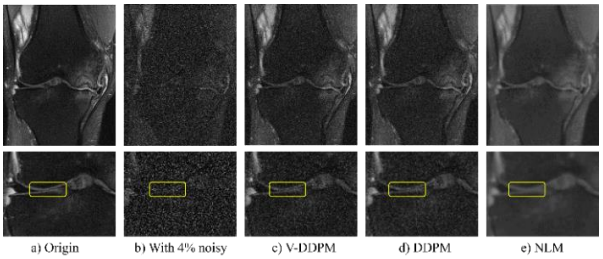

Fig. 5: Comparison of experiment results on Knee MRI. The initial row showcases the entire image, while the subsequent row presents an **amplified** version of the identical region. A comprehensive comparison of detailed information is evident within the designated **yellow box** area.

6. CONCLUSION

In conclusion, we propose an algorithm, V-DDPM, that combines VST and DDPM in this paper. Given that the noise present in MRI scans follows a Rician distribution, it can be observed that the Rician noise conforms to a Rayleigh distribution under low SNR and adheres to a Gaussian distribution under high SNR. First, the MR data containing noise is subjected to VST to approximate the noise to Gaussian noise, then it is denoised by the DDPM algorithm, and finally undergoes IVST to generate a denoised image. Theoretical analysis and experimental results verify that the V-DDPM algorithm can efficiently remove Rician noise from MRI when the noise content is low and can effectively protect the image details and edge information. Compared with other algorithms, the PSNR and SSIM values of the V-DDPM algorithm are improved, and the effect is more easily observed visually. This result confirms that the present algorithm offers some advantages for dealing with Rician noise in medical MRI.

7. ACKNOWLEDGEMENTS

This work was supported by Natural Science Foundation of China (Project No. 62376252, No. 61976196) and Zhejiang Provincial Natural Science Foundation of China (Project No. LZ22F030003).

8. REFERENCES

[1] Mohan, J. et al. "A survey on the magnetic resonance image denoising methods." Biomed. Signal Process. control. 9 (2014): 56- 69.

[2] Sagar, Prof., Ashruti Upadhyaya, Sudhansu Kumar Mishra, Rudra Narayan Pandey, Sitanshu Sekhar Sahu and Ganapati Panda. “A Circular Adaptive Median Filter for Salt and Pepper Noise Suppression from MRI Images.” Journal of Scientific & Industrial Research (2020): n. pag.

[3] A. -K. Seghouane, "Robust Structured Dictionary Learning For Block Sparse Representations Using α-Divergence," 2020 IEEE International Conference on Image Processing (ICIP), Abu Dhabi, United Arab Emirates, 2020, pp. 843-847, doi: 10.1109/ICIP40778.2020.9190984.

[4] A. M. Rekavandi, A. -K. Seghouane and K. Abed-Meraim, "TRPAST: A Tunable and Robust Projection Approximation Subspace Tracking Method," in IEEE Transactions on Signal Processing, vol. 71, pp. 2407-2419, 2023, doi: 10.1109/TSP.2023.3289699.

[5] Chen, Z., Zhou, Z. & Adnan, S. Joint low-rank prior and difference of Gaussian filter for magnetic resonance image denoising. Med Biol Eng Comput 59, 607–620 (2021).

[6] Sharma, A., Chaurasia, V. MRI denoising using advanced NLM filtering with non-subsampled shearlet transform. SIViP 15, 1331–1339 (2021).

[7] Sahu, S., Anand, A., Singh, A.K. et al. MRI de-noising using improved unbiased NLM filter. J Ambient Intell Human Comput 14, 10077–10088 (2023).

[8] Yu, Li-Ling, et al. " Estimation of Rician noise level field and its application in MR image denoising." Chinese Journal of Biomedical Engineering 32.05 (2013): 532-538.

[9] Jiang, Dongsheng et al. “Denoising of 3D magnetic resonance images with multi-channel residual learning of convolutional neural network.” Japanese Journal of Radiology 36 (2017): 566-574.

[10] Ran, Maosong et al. “Denoising of 3D magnetic resonance images using a residual encoder-decoder Wasserstein generative adversarial network.” Medical image analysis 55 (2019): 165-180 .

[11] J. Ho, A. Jain, and P. Abbeel, "Denoising diffusion probabilistic models," Advances in Neural Information Processing Systems, vol. 33, pp. 6840-6851, 2020.

[12] Gregory, Stephen et al. “HydraNet: a multi-branch convolutional neural network architecture for MRI denoising.” Medical Imaging (2021).

[13] A. Lugmayr, M. Danelljan, A. Romero, F. Yu, R. Timofte, and L. Van Gool, "Repaint: Inpainting using denoising diffusion probabilistic models," in Proceedings of the IEEE/CVF Conference on Computer Vision and Pattern Recognition, pp. 11461-11471, 2022.

[14] Nowak, Robert D. "Wavelet-based Rician noise removal for magnetic resonance imaging." IEEE transactions on image processing : a publication of the IEEE Signal Processing Society 8 10 (1999): 1408-19 .

[15] Foi, Alessandro. "Noise estimation and removal in MR imaging: the variance-stabilization approach." 2011 IEEE International Symposium on Biomedical Imaging: From Nano to Macro (2011): 1809-1814.

[16] Henkelman, R. Mark. "Measurement of signal intensities in the presence of noise in MR images." medical physics 12 2 (1985). 232-3 .

[17] Gudbjartsson, Hakon and Samuel Patz. "The rician distribution of noisy mri data. "Magnetic Resonance in Medicine 34 (1995). n. pag.

[18] Knoll, Florian et al. “fastMRI: A Publicly Available Raw k-Space and DICOM Dataset of Knee Images for Accelerated MR Image Reconstruction Using Machine Learning.” Radiology. Artificial intelligence vol. 2,1 e190007. 29 Jan. 2020, doi:10.1148/ryai.2020190007.

[19] Zbontar, Jure et al. “fastMRI: An Open Dataset and Benchmarks for Accelerated MRI.” ArXiv abs/1811.08839 (2018): n. pag.

[20] Wang, Zhou et al. “Image quality assessment: from error visibility to structural similarity.” IEEE Transactions on Image Processing 13 (2004): 600-612.